J. Fluid Mech. (1974), *vol.* 65, *part* 2, *pp.* 209–229
Printed in Great Britain

Natural convection in a shallow cavity with differentially heated end walls. Part 1. Asymptotic theory

By D. E. CORMACK, L. G. LEAL
Chemical Engineering, California Institute of Technology, Pasadena
AND J. IMBERGER
Department of Mathematics and Mechanical Engineering, University of Western Australia, Nedlands

(Received 23 March 1973 and in revised form 15 February 1974)

The problem of natural convection in a cavity of small aspect ratio with differentially heated end walls is considered. It is shown by use of matched asymptotic expansions that the flow consists of two distinct regimes: a parallel flow in the core region and a second, non-parallel flow near the ends of the cavity. A solution valid at all orders in the aspect ratio A is found for the core region, while the first several terms of the appropriate asymptotic expansion are obtained for the end regions. Parametric limits of validity for the parallel flow structure are discussed. Asymptotic expressions for the Nusselt number and the single free parameter of the parallel flow solution, valid in the limit as $A \to 0$, are derived.

1. Introduction

Convection due to buoyancy forces is an important and often dominant mode of heat and mass transport. Of particular significance to the dispersion of pollutants and heat waste in estuaries are the buoyancy-driven convective motions induced by gradients in salt concentration or temperature.

Unfortunately the direct modelling of these natural systems is very complex, mainly because the flow is turbulent. However, the idealized problem of laminar flow in an enclosed rectangular cavity with differentially heated ends does provide some insight into these more difficult problems, and has been studied extensively in other contexts by prior investigators. The majority of these studies have used finite-difference numerical solutions of the full equations of motion, subject to the Boussinesq approximation, to consider cavities which were either square or had height h larger than their length l (cf. Quon 1972; Wilkes & Churchill 1966; Newell & Schmidt 1970; Szekely & Todd (1971); De Vahl Davis 1968). However, Batchelor (1954), Elder (1965) and Gill (1966) have shown that analytical progress is possible when the cavity aspect ratio h/l is large.

Batchelor (1954) considered both large and small Grashof numbers Gr. In the latter case, he obtained an asymptotic solution about the pure conduction

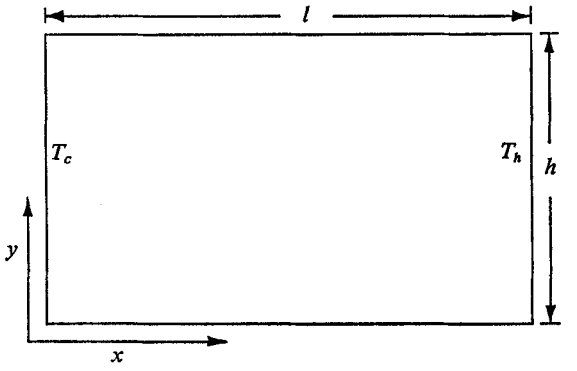

FIGURE 1. Schematic diagram of system.

mode of heat transfer. For large Gr, Batchelor envisaged a flow with thin boundary layers on all solid surfaces and a closed-streamline isothermal core of constant vorticity. Motivated by the experimental measurements of Elder (1965), Gill (1966) proposed an alternative structure for the case $h/l \gg 1$ and $Gr \gg 1$. In Gill's model the flow is decomposed into boundary layers adjacent to the end walls in which the horizontal temperature gradients are large, and a core region in which the temperature is assumed to be a function only of the vertical coordinate. In spite of the approximations necessary to solve the resulting equations Gill reported moderate agreement with the experimental measurements of Elder (1965). A key feature of the case $h/l \gg 1$, which is implicit in Gill's model, is that the core dynamics play only a secondary role in establishing the overall flow structure, which is dominated by the buoyancy-driven boundary layers. A natural question is whether this qualitative feature persists as the aspect ratio h/l is varied. In particular, in the limit as $h/l \to 0$, which is most relevant for the naturally occurring flows of interest in the present investigation, one might anticipate that viscous effects in the core would play an increasingly important role in establishing the flow structure for all fixed (though large) values of Gr.

In the present paper, we use the standard methods of matched asymptotic expansions to consider the cavity flow problem in this limiting case $h/l \ll 1$, Gr fixed. We shall show that the flow structure consists of two parts: a parallel-flow core region in which essentially all of the horizontal temperature drop occurs and which is dominated by viscous effects; and end regions which serve primarily to turn the core flow through 180° as required by the solid end walls. The numerical and experimental results reported in parts 2 and 3 of the present study show excellent agreement with this asymptotic theory for large, though finite values of of $(h/l)^{-1}$.

2. Mathematical formulation of the problem

We consider a closed rectangular two-dimensional cavity of length l and height h which contains a Newtonian fluid, and is shown schematically in figure 1. The end walls are held at different but uniform temperatures T_c and T_h, with $T_c < T_h$.

The top and bottom are insulated, and all surfaces are rigid no-slip boundaries. Actually, the upper boundary of the environmental systems mentioned in the introduction is more closely approximated as a zero-shear surface. However, it was found that the experimental measurements, to be presented in part 3, could be obtained only in a cavity with a no-slip lid. Hence, the present analysis was undertaken to provide a solution that could be compared directly with the experimental results. A systematic investigation of the influence of the upper surface conditions on flow structure may be found in Cormack, Stone & Leal (1974).

The appropriate governing equations, subject to the usual Boussinesq approximations, are

$$\frac{\partial u'}{\partial t'}+u'\frac{\partial u'}{\partial x'}+v'\frac{\partial u'}{\partial y'}=-\frac{1}{\rho_0}\frac{\partial P}{\partial x'}+\nu(\nabla^2 u'), \tag{1}$$

$$\frac{\partial v'}{\partial t'}+u'\frac{\partial v'}{\partial x'}+v'\frac{\partial v'}{\partial y'}=-\frac{1}{\rho_0}\frac{\partial P}{\partial y'}+\nu(\nabla^2 v')+g\beta(T-T_c), \tag{2}$$

$$\partial u'/\partial x'+\partial v'/\partial y'=0, \tag{3}$$

$$\frac{\partial T}{\partial t'}+u'\frac{\partial T}{\partial x'}+v'\frac{\partial T}{\partial y'}=\frac{k}{C_p\rho_0}(\nabla^2 T), \tag{4}$$

with corresponding boundary conditions

$$\begin{aligned} u' = v' &= 0 \quad \text{on all solid boundaries,}\\ \partial T/\partial y' &= 0 \quad \text{on} \quad y'=0,h,\\ T &= T_c, T_h \quad \text{on} \quad x'=0,l. \end{aligned} \tag{5}$$

Here, u' and v' are the horizontal and vertical velocity components; ν, ρ_0, C_p, k and β are the kinematic viscosity, density, heat capacity, thermal conductivity and coefficient of thermal expansion, all referred to some mean temperature of the fluid.

Non-dimensionalizing, using the definitions

$$x=\frac{x'}{h},\quad y=\frac{y'}{h},\quad u=\frac{u'}{g\beta h^3(T_h-T_c)/\nu l},\quad v=\frac{v'}{g\beta h^3(T_h-T_c)/\nu l},$$
$$\theta=(T-T_c)/(T_h-T_c),\quad t=t'g\beta h^2(T_h-T_c)/\nu l,$$

and introducing a stream function ψ such that

$$u=\partial\psi/\partial y,\quad v=-\partial\psi/\partial x,$$

one can reduce (1)–(4) to

$$GrA^2\left(\frac{\partial\omega}{\partial t}+\frac{\partial(\omega,\psi)}{\partial(x,y)}\right)=A\nabla^2\omega+\frac{\partial\theta}{\partial x}, \tag{6}$$

$$\nabla^2\psi=-\omega. \tag{7}$$

$$GrPrA\left(\frac{\partial\theta}{\partial t}+\frac{\partial(\theta,\psi)}{\partial(x,y)}\right)=\nabla^2\theta, \tag{8}$$

with boundary conditions

$$\psi=\partial\psi/\partial x=0,\quad \theta=Ax \quad \text{at} \quad x=0,A^{-1} \tag{9a}$$

and

$$\psi=\partial\psi/\partial y=\partial\theta/\partial y=0 \quad \text{at} \quad y=0,1. \tag{9b}$$

Although the characteristic velocity scaling may at first appear an arbitrary choice, it is consistent with the physical picture of a buoyancy-driven parallel flow which is moderated by viscous effects over a length l, and may in fact be justified *a posteriori* by the theory which is presented in this paper. The dimensionless parameters are

$$Gr \equiv g\beta(T_h - T_c)\, h^3/\nu^2 \quad \text{(Grashof number)},$$

$$Pr \equiv C_p \mu/k \quad \text{(Prandtl number)}$$

and

$$A \equiv h/l \quad \text{(aspect ratio)}.$$

In what follows, we consider the asymptotic problem in which $A \to 0$ with Pr and Gr held fixed.

3. The core flow

The key to a proper asymptotic solution, in the present case, is a proper resolution of the central or core region of the cavity. Fortunately, the flow structure in this region is surprisingly simple and amenable to direct analytical solution of the governing equations. Both the numerical and experimental evidence which we shall present in parts 2 and 3 in fact indicate that the streamlines in the core region become more nearly parallel as the aspect ratio is decreased, with substantial deviations from this structure only occurring in the immediate vicinity of the end walls. Acceptance of a parallel flow structure as a first approximation in the core would imply that the appropriate characteristic scale length in the x direction must be $O(A^{-1})$.

With introduction of the characteristic horizontal scale $x = O(A^{-1})$, equations (6)–(8) become

$$Gr\, A^2 \frac{\partial(\omega, \psi)}{\partial(\hat{x}, y)} = A^2 \frac{\partial^2 \omega}{\partial \hat{x}^2} + \frac{\partial^2 \omega}{\partial y^2} + \frac{\partial \theta}{\partial \hat{x}}, \tag{10}$$

$$A^2 \partial^2 \psi / \partial \hat{x}^2 + \partial^2 \psi / \partial y^2 = -\omega, \tag{11}$$

$$Pr\, Gr\, A^2 \frac{\partial(\theta, \psi)}{\partial(\hat{x}, y)} = A^2 \frac{\partial^2 \theta}{\partial \hat{x}^2} + \frac{\partial^2 \theta}{\partial y^2}, \tag{12}$$

where $\hat{x} = Ax$.

Using (10)–(12), one may now obtain the full asymptotic solution for the core temperature and velocity fields, as a regular expansion in the small parameter A. Although the precise forms of the gauge functions in this expansion are strictly obtainable only from the requirements for a proper asymptotic match with the corresponding solutions in the end regions, we anticipate the simple form (which will be verified *a posteriori*)

$$\left.\begin{aligned} \theta &= \theta_0 + A\theta_1 + A^2\theta_2 + \dots, \\ \psi &= \psi_0 + A\psi_1 + A^2\psi_2 + \dots, \\ \omega &= \omega_0 + A\omega_1 + A^2\omega_2 + \dots. \end{aligned}\right\} \tag{13}$$

The systematic solution, valid for $A \ll 1$, which results on substituting these

expansions into (10)–(12) and equating terms of like order in A has the same form at all orders in A, i.e.

$$\psi = K_1(\tfrac{1}{24}y^4 - \tfrac{1}{12}y^3 + \tfrac{1}{24}y^2), \tag{14}$$

$$\theta = K_1\hat{x} + K_1^2 Gr\,Pr\,A^2(\tfrac{1}{120}y^5 - \tfrac{1}{48}y^4 + \tfrac{1}{72}y^3) + K_2, \tag{15}$$

where

$$K_1 = c_1 + c_2 A + c_3 A^2 + \ldots,$$

$$K_2 = c_1^* + c_2^* A + c_3^* A^2 \ldots$$

and $c_1, c_2, \ldots, c_1^*, c_2^*, \ldots, c_n^*$ are constants which depend on Gr and Pr.

The velocity field corresponding to (14) is strictly parallel to the top and bottom walls of the cavity, and cannot, therefore, satisfy the boundary conditions ($9a$) at the end walls. These conditions must be satisfied by solutions valid in the end regions, and in general, the two parameters K_1 and K_2 are evaluated by matching the core solution with these two end-region solutions. In the present case, however, the problem simplifies somewhat owing to the centro-symmetry property of the equations and boundary conditions (discussed by Gill 1966). This property imposes the requirement on the solutions that

$$\psi(\hat{x}, y) = \psi(1-\hat{x}, 1-y), \quad \omega(\hat{x}, y) = \omega(1-\hat{x}, 1-y)$$

and

$$\theta(\hat{x}, y) = 1 - \theta(1-\hat{x}, 1-y).$$

Hence, one half of the cavity is an inverted mirror image of the other. Moreover, it is apparent that

$$\theta(\tfrac{1}{2}, \tfrac{1}{2}) = \tfrac{1}{2},$$

so that, according to (15),

$$\tfrac{1}{2}K_1 + \tfrac{1}{1440}K_1^2 Gr\,Pr\,A^2 + K_2 = \tfrac{1}{2}.$$

This relationship allows the constants c_i^* (and hence K_2) to be entirely eliminated in favour of the single set $\{c_i\}, i = 1, 2, \ldots, \infty$, e.g.

$$c_1^* = \tfrac{1}{2} - \tfrac{1}{2}c_1, \quad c_2^* = -\tfrac{1}{2}c_2, \quad c_3^* = -\tfrac{1}{2}c_3 - \tfrac{1}{1440}c_1^2 Gr\,Pr. \tag{16a, b, c}$$

With the constant K_2 thus eliminated, it is possible to evaluate K_1 completely (and hence the $c_i, i = 1, 2, \ldots, \infty$, which depend on Gr and Pr) by matching the core solution with a proper solution that is valid in either of the two end regions. This matching process is, of course, considerably simplified by the fact that the basic form of the core solution is preserved at all orders in the small parameter A.

Before proceeding to a resolution of the flow in the end regions, it is useful to note the key structural features of the basic core solution for Gr fixed, $A \to 0$ [equations (14) and (15)] and to contrast these with the structure in the previously noted conduction and boundary-layer limits A fixed, $Gr \to 0$ and A fixed, $Gr \to \infty$ of Batchelor and Gill. The solution (14) and (15) exhibits two key features. First, the velocity field in the core is parallel to all orders in the small parameter A. Second, to a first approximation, θ is independent of vertical position, and varies linearly between the end walls. The primary driving force for motion is the horizontal temperature gradient in the core. In fact, we shall show in the next section that $c_1 = 1$, so that effectively all of the temperature drop

occurs across the core. The end regions are thus dynamically passive, in the sense that they serve simply to turn the flow through 180° as required by the condition of zero volume flux through the end walls. In contrast, for the boundary-layer limit A fixed, $Gr \to \infty$ considered by Gill, nearly all of the temperature drop occurs in thin layers at the two ends, and these provide the driving force for flow. In this case, it is the *core* region which is passive. Flow exists there only as a result of entrainment–detrainment from the end-wall boundary layers. Clearly, the flow structure for A fixed (perhaps small), $Gr \to \infty$ is fundamentally different from that for Gr fixed (perhaps large), $A \to 0$.

It is obvious from the first-order temperature distribution that the heat transfer process is dominated by conduction. Thus, it is important to note that the present theory is definitely distinct from the pure conduction limit A fixed, $Gr \to 0$ considered by Batchelor. Physically, the dominance of conduction for asymptotically small values of A (with Gr large) is a result of the cumulative effect of locally small viscous effects acting over a sufficiently long distance. This reasoning is also consistent with the velocity scaling, which indicates that the length of the cavity plays a role that is identical with that played by viscosity. That is, by either doubling the length or doubling the viscosity, while keeping all other variables constant, one achieves the same effect, to cut the core velocity in half. Hence, when A is small enough, the core velocity is actually 'throttled' to small magnitude by viscosity for any arbitrarily large value of Gr.

4. The flow in the end regions

We turn now to a consideration of the end regions of the cavity where the core flow described in the previous section is not valid. Although we are primarily interested in determining the coefficients c_i of the parameter K_1, and hence the quantitative details of the core region, it is nevertheless of some interest to develop the full asymptotic solution in this region of the flow. In view of the centrosymmetry of the problem, we explicitly consider only the end $x = 0$. As we shall see, it is necessary to proceed to third order in the end flow solution in order to obtain the first non-trivial correction for the core region.

In the end regions, the characteristic length scales in each of the co-ordinate directions are $O(h)$. In this sense, the structure for $A \to 0$, Gr fixed (and large) is fundamentally different from the expected structure for $Gr \to \infty$, with A fixed (and small), since there exist no boundary-layer-like regions in the present case. Furthermore, since the parallel structure of the core requires that *all* streamlines eventually enter the end region, it is clear that the scaling used for the horizontal velocity in the core must be maintained in the analysis of the end regions. Hence, (6)–(8) must be solved subject to the boundary conditions

$$\psi = \partial\psi/\partial y = \partial\theta/\partial y = 0 \quad \text{on} \quad y = 0, 1, \tag{17a}$$

$$\psi = \partial\psi/\partial x = \theta = 0 \quad \text{on} \quad x = 0 \tag{17b}$$

and the matching condition

$$\lim_{x\to\infty} \psi_{\text{end}}(x, y) \Leftrightarrow \lim_{\hat{x}\to 0} \psi_{\text{core}}(\hat{x}, y) \quad \text{as} \quad A \to 0. \tag{18}$$

As in the core region, the solution can be obtained as a regular perturbation expansion in the small parameter A of the form

$$\theta = \theta_0 + A\theta_1 + A^2\theta_2 + \ldots,$$
$$\psi = \psi_0 + A\psi_1 + A^2\psi_2 + \ldots,$$
$$\omega = \omega_0 + A\omega_1 + A^2\omega_2 + \ldots.$$

Substituting these expansions into (6)–(8) and equating terms of like order in A, we obtain an infinite sequence of coupled linear differential equations for the unknown functions θ_i, ψ_i and ω_i. In order to clarify the discussion to follow, we list these together with the explicit matching conditions which must be satisfied for large x, up to $O(A^3)$.

(i) At $O(1)$

$$\partial\theta_0/\partial x = 0,$$
$$\nabla^2\theta_0 = 0, \quad \lim_{x\to\infty}\theta_0 = c_1^*. \tag{19}$$

(ii) At $O(A)$

$$\nabla^2\omega_0 = -\partial\theta_1/\partial x, \quad \nabla^2\psi_0 = -\omega_0, \tag{20}$$
$$\nabla^2\theta_1 = Pr\,Gr\,\partial(\theta_0,\psi_0)/\partial(x,y), \tag{21}$$
$$\lim_{x\to\infty}\psi_0 = c_1(\tfrac{1}{24}y^4 - \tfrac{1}{12}y^3 + \tfrac{1}{24}y^2),$$
$$\lim_{x\to\infty}\partial\psi_0/\partial x = 0, \quad \lim_{x\to\infty}\theta_1 - c_1 x + c_2^*.$$

(iii) At $O(A^2)$

$$\nabla^2\omega_1 + \partial\theta_2/\partial x = Gr\,\partial(\omega_0,\psi_0)/\partial(x,y), \tag{22}$$
$$\nabla^2\psi_1 = -\omega_1,$$
$$\nabla^2\theta_2 = Pr\,Gr\left(\frac{\partial(\theta_1,\psi_0)}{\partial(x,y)} + \frac{\partial(\theta_0,\psi_1)}{\partial(x,y)}\right), \tag{23}$$
$$\lim_{x\to\infty}\psi_1 = c_2(\tfrac{1}{24}y^4 - \tfrac{1}{12}y^3 + \tfrac{1}{24}y^2),$$
$$\lim_{x\to\infty}\partial\psi_1/\partial x = 0, \quad \lim_{x\to\infty}\theta_2 = c_2 x + c_1^2 Gr\,Pr\,(\tfrac{1}{120}y^5 - \tfrac{1}{48}y^4 + \tfrac{1}{72}y^3) + c_3^*.$$

(iv) At $O(A^3)$

$$\nabla^2\omega_2 + \frac{\partial\theta_3}{\partial x} = Gr\left(\frac{\partial(\omega_0,\psi_1)}{\partial(x,y)} + \frac{\partial(\omega_1,\psi_0)}{\partial(x,y)}\right), \tag{24}$$
$$\nabla^2\psi_2 = -\omega_2,$$
$$\nabla^2\theta_3 = Pr\,Gr\left(\frac{\partial(\theta_1,\psi_1)}{\partial(x,y)} + \frac{\partial(\theta_2,\psi_0)}{\partial(x,y)} + \frac{\partial(\theta_0,\psi_2)}{\partial(x,y)}\right), \tag{25}$$
$$\lim_{x\to\infty}\psi_2 = c_3(\tfrac{1}{24}y^4 - \tfrac{1}{12}y^3 + \tfrac{1}{24}y^2),$$
$$\lim_{x\to\infty}\partial\psi_2/\partial x = 0, \quad \lim_{x\to\infty}\theta_3 = c_3 x + 2c_1 c_2\,Gr\,Pr\,(\tfrac{1}{120}y^5 - \tfrac{1}{48}y^4 + \tfrac{1}{72}y^3) + c_4^*.$$

The boundary conditions (17a, b) at each order become simply

$$\psi_i = \partial\psi_i/\partial y = \partial\theta_i/\partial y = 0 \quad \text{on} \quad y = 0, 1, \tag{26a}$$
$$\psi_i = \partial\psi_i/\partial x = \theta_i = 0 \quad \text{on} \quad x = 0. \tag{26b}$$

The temperature and velocity fields θ_0, θ_1, ψ_0 and ω_0

We begin by considering the $O(1)$ and $O(A)$ fields using (19)–(21). The solution at $O(1)$ for θ_0 is trivial, since the only solution of $\partial\theta_0/\partial x = 0$ which satisfies the boundary conditions (26) is $\theta_0 \equiv 0$. It follows from the matching condition

and (16*a*) that $c_1^* = 0$ and $c_1 = 1$. Moreover, substitution of this solution into (21) gives $\nabla^2\theta_1 = 0$. With the appropriate boundary and matching conditions, this leads to the solution $\theta_1 = x$, from which it follows that $c_2^* = c_2 = 0$. Hence to first order, the temperature distribution everywhere in the cavity is strictly linear in x and the dominant mode of heat transfer is pure conduction. In this limited sense the present solution resembles the earlier work of Batchelor for $Gr \ll 1$ and A fixed, though it should be re-emphasized that the present analysis is valid for any Gr provided only that A is sufficiently small.†

In the light of the above results, (20) may be rewritten as

$$\nabla^2\omega_0 = -1, \quad \nabla^2\psi_0 = -\omega_0. \tag{27}$$

In view of the previously stated matching conditions for ψ_0, it is convenient to introduce the transformation

$$\psi_0 = \phi + (\tfrac{1}{24}y^4 - \tfrac{1}{12}y^3 + \tfrac{1}{24}y^2)$$

into (27), which may then be combined to give

$$\nabla^4\phi = 0, \tag{28}$$

with the boundary conditions

$$\phi = \partial\phi/\partial y = 0 \quad \text{on} \quad y = 0, 1,$$
$$\phi = -(\tfrac{1}{24}y^4 - \tfrac{1}{12}y^3 + \tfrac{1}{24}y^2), \quad \partial\phi/\partial x = 0 \quad \text{on} \quad x = 0.$$

The required matching with the core solution yields the final boundary condition on ϕ,

$$\lim_{x\to\infty} \phi = \lim_{x\to\infty} \partial\phi/\partial x = 0.$$

The distribution of ϕ is identical with the displacement of an elastic semi-infinite strip clamped at the edges and subjected to a small displacement at $x = 0$. The difficulties inherent in obtaining an analytic solution to problems of this general nature are well known. On the other hand, numerical solution can be rather straightforward and would be sufficient in the present case for generating an accurate approximation to the stream-function field in the end region. Nevertheless, we feel that it is worthwhile to pursue the analytical representation since the method of solution is interesting in its own right. Furthermore, it provides a useful check on the numerical solution for ψ_0 that is to be used in subsequent stages of the asymptotic theory.

To obtain an analytical expression for ϕ, we extend a method developed by Benthem (1963) that largely follows the well-known lines of Laplace transform theory. If new independent variables are defined as

$$y' = 2y - 1, \quad x' = 2x,$$

so that ϕ is even in y', then the boundary function $\phi(0, y')$ may be expanded as a cosine series

$$\phi(0, y') = \sum_{n=1}^{\infty} d_n \cos\left(\frac{n\pi}{2} y'\right), \tag{29}$$

with

$$d_n = 2\sin\left(\frac{n\pi}{2}\right)(1 - (-1)^n)\left(\frac{1}{12n^3\pi^3} - \frac{1}{n^5\pi^5}\right). \tag{30}$$

† A more explicit condition for validity of the present theory will appear in §5.

k	$2s_k$
1	$4{\cdot}2124+i\ 2{\cdot}2507$
2	$10{\cdot}7125+i\ 3{\cdot}1032$
3	$17{\cdot}0734+i\ 3{\cdot}5511$
4	$23{\cdot}3984+i\ 3{\cdot}8588$

TABLE 1. First four roots of $\sin 2s_i + 2s_i = 0$ in first quadrant

The key to obtaining an analytical solution is the assumption that the second- and third-order derivatives of ϕ on the boundary may also be expressed as cosine series of the similar form

$$\left.\frac{\partial^2\phi}{\partial x'^2}\right|_{x'=0} = \sum_{n=1}^{\infty} a_n \cos\left(\frac{n\pi}{2}y'\right) \tag{31}$$

and

$$\left.\frac{\partial^3\phi}{\partial x'^3}\right|_{x'=0} = \sum_{n=1}^{\infty} b_n \cos\left(\frac{n\pi}{2}y'\right), \tag{32}$$

where a_n and b_n are unknown coefficients to be determined. Following the familiar procedures of Laplace transform theory and after considerable manipulation, the solution may ultimately be expressed as an expansion in Papkowich–Fadle eigenfunctions (cf. Fadle 1941)

$$\phi(x',y') = \sum_{k=1}^{\infty}\sum_{n=1}^{\infty}\left[\frac{d_n(-s_k^3+\frac{1}{2}n\pi s_k)-a_n s_k+b_n}{(s_k^2-(\frac{1}{2}n\pi)^2)^2}-\frac{d_n}{s_k}\right]\frac{n\pi\sin\frac{1}{2}n\pi}{4\cos^2 s_k} \times(\sin s_k\cos s_k y'-y'\cos s_k\sin s_k y')\,e^{-s_k x'}, \tag{33}$$

where $s_k, k = 1, 2, \ldots, \infty$, are the complex roots (with positive real part) of the transcendental equation

$$\sin 2s_k + 2s_k = 0 \tag{34}$$

and a_n and b_n satisfy the set of algebraic equations

$$\sum_{n=1}^{\infty}\left\{\frac{d_n(s_k^3-\frac{1}{2}n\pi s_k)+a_n s_k+b_n}{(s_k^2-(\frac{1}{2}n\pi)^2)^2}-\frac{d_n}{s_k}\right\}n\pi\sin\tfrac{1}{2}n\pi = 0, \quad k = 1,2,\ldots,\infty. \tag{35}$$

In theory, the determination of a_n and b_n requires the inversion of a matrix of infinite dimension. Hence, in practice one must truncate the series after a finite number of terms (assume that the rest are zero) and obtain an approximate solution.

The first four roots of the transcendental equation (34) that occur in the first quadrant of the imaginary plane have been tabulated by Mittleman & Hillman (1946) and are listed in table 1. Furthermore, if $q+ir$ is an eigenvalue, then so is $q-ir$ since the roots of (34) are symmetrically placed about both the real and imaginary axes. This symmetry ensures that the imaginary part of (33) is identically zero.

We were unable to prove analytically that the truncated approximation of (33) converges to the correct solution of (28). However, a qualitative indication of such convergence is provided by a comparison of truncated versions of (33) with a full numerical solution of the governing equations plus associated

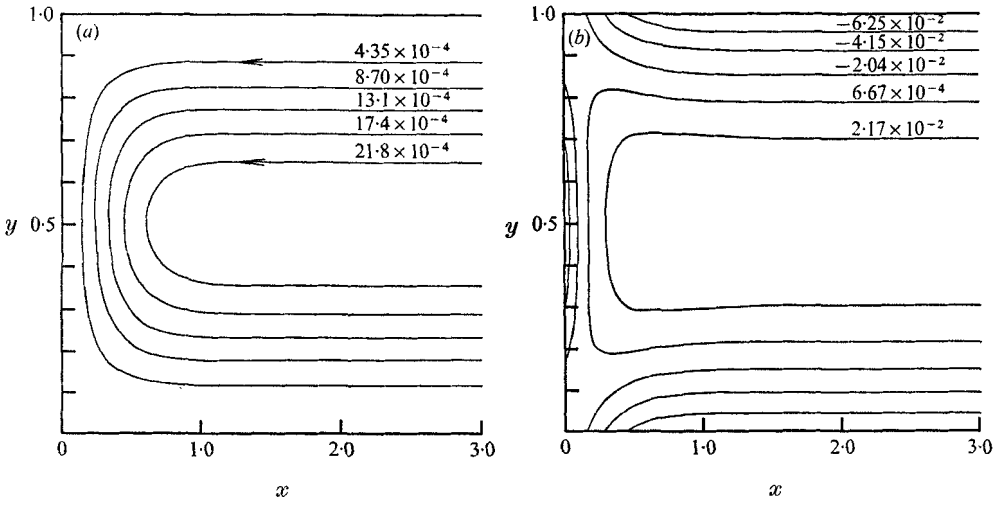

FIGURE 2. (*a*) First-order stream function ψ_0 (streamlines) and (*b*) first-order vorticity ω_0 (lines of constant vorticity).

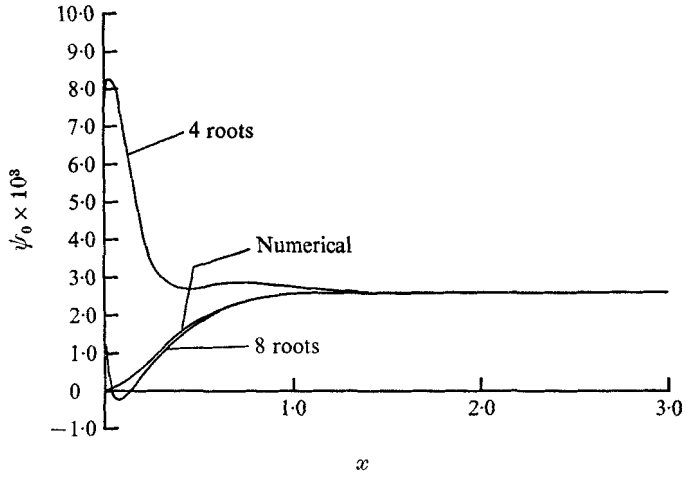

FIGURE 3. Comparison of numerical and analytical solutions for ψ_0.

boundary conditions. A numerical solution of (27) was therefore obtained for ψ_0 and ω_0 by means of an explicit Gauss–Seidel iteration scheme. The equations were approximated by a central difference representation on a geometrically expanding grid of 21 points in the x direction and a sine-transformed grid of 21 points in the y direction (a similar sine-transformed grid will be described in part 2). The boundary conditions at $x = \infty$ were applied at the finite distance $x = 3$. All of these numerical parameters were systematically varied to demonstrate their adequacy for the present purposes. The numerically determined streamlines and equi-vorticity lines are plotted in figures 2 (*a*) and (*b*). Although we shall subsequently discuss some qualitative features of these plots, we first return to the comparison of the numerical and analytical solutions.

		4 roots		8 roots	
n	d_n	a_n	b_n	a_n	b_n
1	$-2{\cdot}307\times10^{-3}$	$5{\cdot}267\times10^{-2}$	$4{\cdot}482\times10^{-1}$	$5{\cdot}620\times10^{-3}$	$1{\cdot}039\times10^{-2}$
3	$-3{\cdot}440\times10^{-4}$	$-5{\cdot}295\times10^{-1}$	$1{\cdot}934\times10^{-1}$	$5{\cdot}842\times10^{-2}$	$-1{\cdot}886\times10^{-1}$
5	$8{\cdot}173\times10^{-5}$	$9{\cdot}866\times10^{-1}$	$3{\cdot}642$	$-7{\cdot}322\times10^{-2}$	$2{\cdot}565\times10^{-1}$
7	$-3{\cdot}053\times10^{-5}$	$5{\cdot}258$	$-3{\cdot}309\times10^{1}$	$3{\cdot}017\times10^{-1}$	$-2{\cdot}451$
9	$1{\cdot}451\times10^{-5}$	—	—	$-1{\cdot}279\times10^{-1}$	$-2{\cdot}254$
11	$-7{\cdot}986\times10^{-6}$	—	—	$-1{\cdot}671\times10^{-1}$	$-6{\cdot}813$
13	$4{\cdot}852\times10^{-6}$	—	—	$2{\cdot}429$	$7{\cdot}409$
15	$-3{\cdot}164\times10^{-6}$	—	—	$7{\cdot}152$	$1{\cdot}581\times10^{1}$

TABLE 2. Values of d_n, a_n and b_n

The required comparison is provided by figure 3, where we have plotted the centre-line values of ψ_0 as a function of x, from the numerical solution and from (33), using both the first four and the first eight available eigenvalues. The solution obtained by using only the first two eigenvalues from each of the first and fourth quadrants represents a rather poor approximation to the 'exact' (numerical) solution. On the other hand, when all eight of the available eigenvalues are used (i.e. eight terms of the infinite series are retained), the correspondence between the numerical and analytical solutions is greatly improved. In fact, appreciable deviations from the numerical solution persist only for $x < 0{\cdot}3$. The coefficients d_n, a_n and b_n corresponding to the four- and eight-term approximations to (33) are listed in table 2. Presumably, inclusion of more terms in the series would improve the comparison of the analytical and numerical solutions. We shall not, however, carry the analysis further in this paper.

The chief feature of interest in the flow field, evident from figure 2, is that both the streamlines and equi-vorticity lines are nearly parallel for $x \geqslant 1$. This observation is consistent with the initial assumption that the horizontal length scale characterizing the end regions is $O(h)$. In addition, it is of some interest to note that the linear gradient of θ_1 acts as a source of positive vorticity in the region away from the walls (figure 2*b*), while the motion of the fluid past the walls produces vorticity of opposite (negative) sign.

The temperature and velocity fields at higher orders of approximation

To obtain the coefficients c_3, c_4, etc. corresponding to higher-order approximations in the core flow, it is necessary to continue to higher orders in the end regions as well. The remainder of this section is concerned with the solution of (22)–(25) for the functions ψ_1, ω_1 and θ_2 and ψ_2, ω_2 and θ_3, which, when combined with the results of the previous section, yield the coefficients c_3 and c_4, respectively.

Although, in theory, it is relatively straightforward to obtain an analytical solution for θ_2, it is impractical in view of the complexity of the solution for ψ_0 to use this or higher-order solutions to evaluate the stream function, vorticity or temperature at any given point. Hence, to determine θ_2, ψ_1 and ω_1, we proceed numerically, using the numerical solutions for ψ_0 and ω_0 in conjunction with

(22) and (23). The explicit dependence on Pr and Gr is eliminated by applying the transformations

$$\theta_2 = Gr\,Pr\,\theta_2', \quad \psi_1 = Pr\,Gr\,\psi_1' + Gr\,\psi_1'', \quad \omega_1 = Pr\,Gr\,\omega_1' + Gr\,\omega_1''$$

to (22) and (23), which become

$$\nabla^4\psi_1' = \partial\theta_2/\partial x, \tag{36a}$$

$$\nabla^4\psi_1'' = -\partial(\omega_0, \psi_0)/\partial(x, y), \tag{36b}$$

$$\nabla^2\theta_2' = \partial\psi_0/\partial y. \tag{37}$$

These equations are to be solved together with the homogeneous boundary conditions (26) and the matching conditions

$$\lim_{x\to\infty}\psi_1' = \lim_{x\to\infty}\partial\psi_1'/\partial x = 0, \tag{38a}$$

$$\lim_{x\to\infty}\psi_1'' = \lim_{x\to\infty}\partial\psi_1''/\partial x = 0 \tag{38b}$$

and

$$\lim_{x\to\infty}\theta_2' = f(y) - \tfrac{1}{2}c_3', \tag{39}$$

where $c_3' = c_3/Pr\,Gr$ and $f(y) = \frac{1}{120}y^5 - \frac{1}{48}y^4 + \frac{1}{72}y^3 - \frac{1}{1440}$.

The coefficient c_3' is easily evaluated by noting that (37), integrated over the depth of the cavity, may be combined with the boundary conditions at $y = 0$, 1 to yield

$$\frac{d^2}{dx^2}\left[\int_0^1 \theta_2'\,dy\right] = 0. \tag{40}$$

The only solution of (40) satisfying the relevant boundary condition

$$\int_0^1 \theta_2'\,dy = 0 \quad \text{at} \quad x = 0$$

and the matching condition $\lim_{x\to\infty}\int_0^1 \theta_2'\,dy = -\frac{c_3'}{2}$

is the trivial solution $\int_0^1 \theta_2'\,dy \equiv 0,$

with the important implication that

$$c_3' \equiv 0. \tag{41}$$

A numerical solution for θ_2' was obtained using the same grid and iterative procedure that were previously used for the determination of ψ_0. The result is shown in figure 4, where lines of constant θ_2' are plotted. The main feature is the strong y dependence of θ_2', which clearly represents a sharp departure from the pure conduction temperature profile obtained for θ_1. While $\partial\theta_2'/\partial x$ is negative for $y < 0{\cdot}5$, it is positive for $y > 0{\cdot}5$. In addition, this solution is consistent with the asymptotic boundary condition since $\partial\theta_2'/\partial x \to 0$ as $x \to \infty$.

Using the numerical solutions for θ_2' and ψ_0, we proceed to the solution for ψ_1 and ω_1. Since ψ_1 is subject only to homogeneous boundary conditions, it

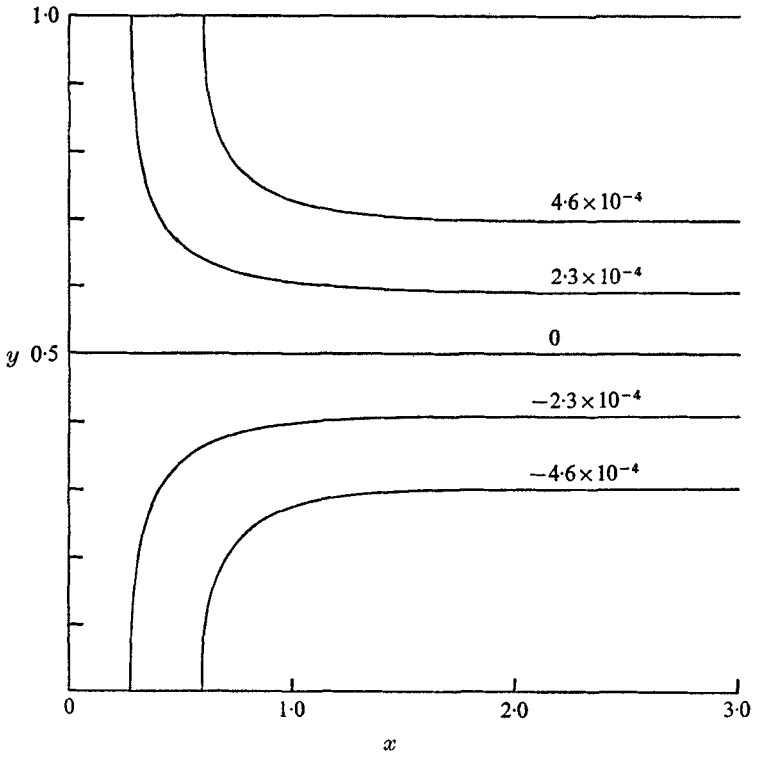

FIGURE 4. $O(A^2)$ temperature correction θ_2': isotherms.

follows that the associated flow is confined to the end region and hence interacts only indirectly with the core flow. Equations (36*a*, *b*) were again solved numerically using the previously described numerical solutions to generate the inhomogeneous terms. The resultant solutions for ψ_1' and ψ_1'' are presented in figures 5(*a*) and (*b*), respectively. As expected, both corrections are characterized by closed streamlines. In the upper half of the end region the contours of positive ψ_1' indicate that the positive gradient of θ_2' induces a counterclockwise flow, whereas in the lower half the converse is true. The streamlines of ψ_1'' are similar to those of ψ_1', but are of opposite sign, and smaller magnitude. The vorticity functions ω_1' and ω_1'' which we have *not* plotted are similar, with closed contours of positive (negative) vorticity in the upper half and of negative (positive) vorticity in the lower half.

We shall return, after first describing the solution for the velocity and temperature fields ψ_2, ω_2 and θ_3, to consider the qualitative influence of ψ_1 on the flow characteristics in the end region.

The $O(A^3)$ problem for ψ_2, ω_2 and θ_3 is simplified considerably by the previous results. Turning first to the temperature equation (25), we note that $\partial(\theta_0, \psi_2)/\partial(x, y)$ is identically zero, while $\partial(\theta_1, \psi_1)/\partial(x, y)$ reduces to $\partial\psi_1/\partial y$. Moreover, one can eliminate the Pr, Gr dependence of the equation by introducing the change of variables

$$\theta_3 = Pr^2 Gr^2 \theta_3' + Pr\, Gr^2 \theta_3''$$

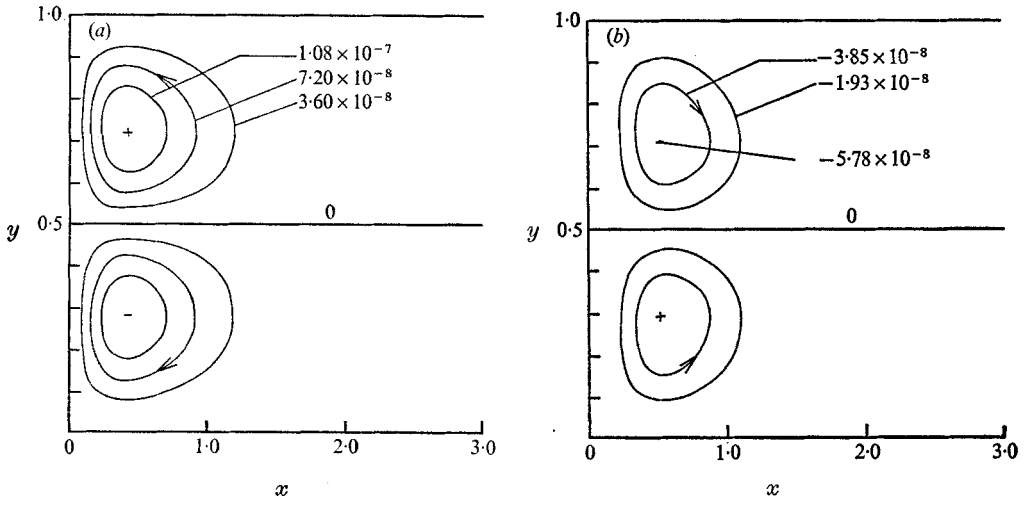

FIGURE 5. (*a*) $O(Gr\,Pr\,A)$ stream function ψ_1' and (*b*) $O(Gr\,A)$ stream function ψ_1'': streamlines.

to yield the independent equations

$$\nabla^2\theta_3' = \partial\psi_1'/\partial y + \partial(\theta_2', \psi_0)/\partial(x, y) \tag{42a}$$

and

$$\nabla^2\theta_3'' = \partial\psi_1''/\partial y, \tag{42b}$$

which must be solved subject to the boundary conditions

$$\theta_3' = \theta_3'' = 0 \quad \text{on} \quad x = 0,$$

$$\partial\theta_3'/\partial y = \partial\theta_3''/\partial y = 0 \quad \text{on} \quad y = 0, 1$$

and the matching conditions

$$\lim_{x\to\infty} \theta_3' = -\tfrac{1}{2}c_4', \quad \lim_{x\to\infty} \theta_3'' = -\tfrac{1}{2}c_4'', \tag{43a, b}$$

where

$$c_4 = Pr^2 Gr^2 c_4' + Pr\,Gr^2 c_4''.$$

The integral of (42*b*) over the depth of the cavity indicates that, like c_3', c_4'' is identically zero. However, the same is not true for c_4'. Hence, this constant must be determined during the course of the numerical solution for θ_3'. This is accomplished by noting that (43*a*) also implies

$$\lim_{x\to\infty} \partial\theta_3'/\partial x = 0. \tag{44}$$

Since the solution of (42*a*) subject to either of the conditions (43*a*) or (44) is unique, the numerical solution of the latter problem not only yields θ_3', but also c_4'. A surprising feature of this solution is that θ_3' appears to depend only on x to within the available numerical accuracy. Hence, in figure 6 we have plotted only the centre-line value for θ_3' as a function of x. It is evident that θ_3' does asymptotically approach a constant value of approximately $1{\cdot}74 \times 10^{-6}$, so that

$$c_4' = -3{\cdot}48 \times 10^{-6}.$$

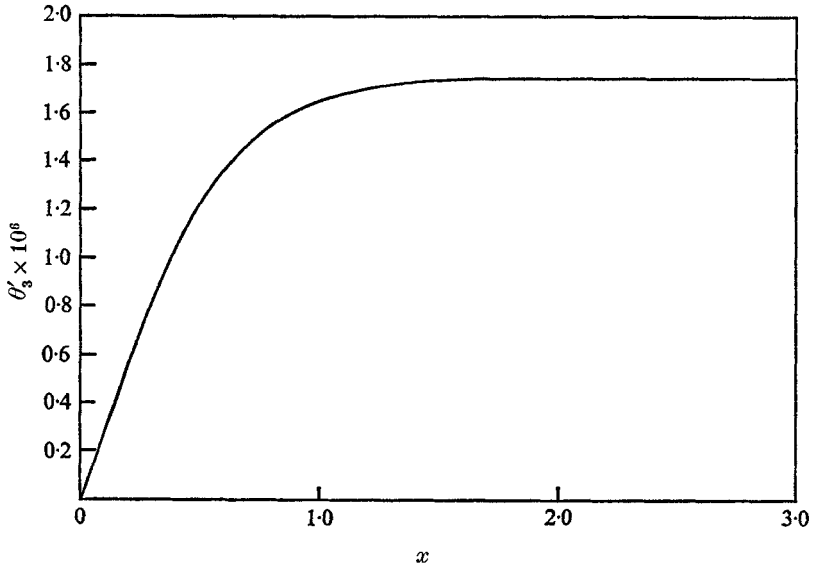

FIGURE 6. $O(Pr^2\, Gr^2\, A^3)$ temperature correction θ_3' *vs.* x.

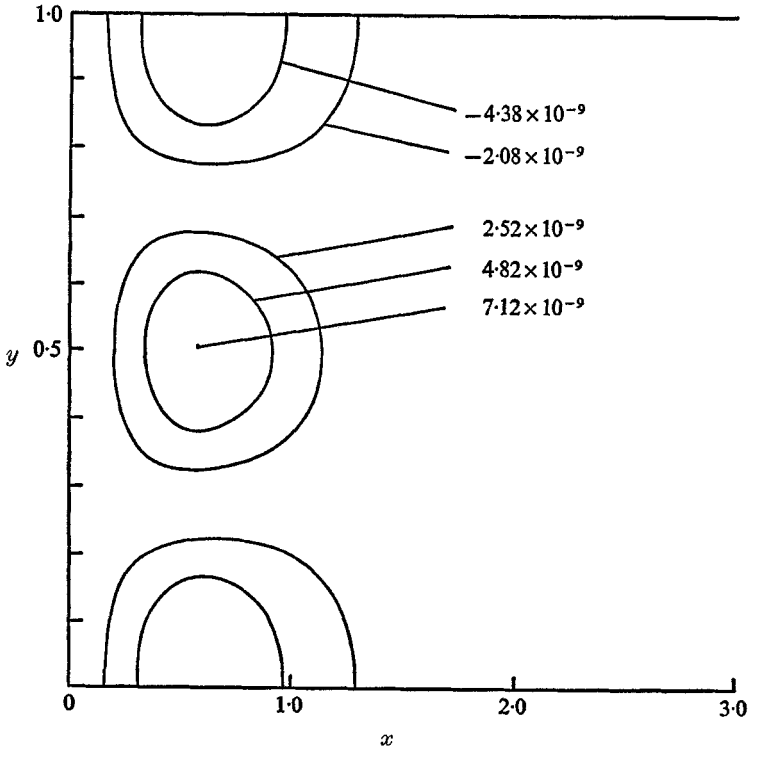

FIGURE 7. $O(Pr\, Gr^2\, A^3)$ temperature correction θ_3'': isotherms.

In contrast to θ_3', the numerical solution for θ_3'', as shown by the contours in figure 7, is a strong function of y. However, since θ_3'' is approximately two orders of magnitude smaller than θ_3', the $O(A^3)$ correction to the temperature field will always be dominated by θ_3' unless $Pr \ll 1$. The fact that c_4' is non-zero is significant because it provides the first correction to K_1 and hence, to the temperature and velocity profiles in the core due to the interaction with the end region. Correct to $O(Gr^2 Pr^2 A^3)$, the constant K_1 is

$$K_1 = 1 - 3{\cdot}48 \times 10^{-6} Gr^2 Pr^2 A^3. \tag{45}$$

Although this correction for K_1 is largely sufficient for providing a comparison between the asymptotic theory presented here and the numerical and experimental results of parts 2 and 3, it is beneficial to obtain one more term of the end-region stream-function expansion, ψ_2, since it provides a detailed flow correction which is very evident in the numerical solutions to be presented in part 2.

Like ψ_1 and ω_1, ψ_2 and ω_2 are subject only to homogeneous boundary conditions. To eliminate the Pr, Gr dependence in (24), it is convenient to break this problem into three parts by means of the transformations

$$\psi_2 = Pr^2 Gr^2 \psi_2' + Pr\, Gr^2 \psi_2'' + Gr^2 \psi_2''',$$
$$\omega_2 = Pr^2 Gr^2 \omega_2' + Pr\, Gr^2 \omega_2'' + Gr^2 \omega_2''',$$

such that

$$\nabla^4 \psi_2' = \partial \theta_3'/\partial x, \tag{46a}$$

$$\nabla^4 \psi_2'' = \frac{\partial \theta_3''}{\partial x} - \frac{\partial(\omega_0, \psi_1')}{\partial(x,y)} - \frac{\partial(\omega_1', \psi_0)}{\partial(x,y)} \tag{46b}$$

and

$$\nabla^4 \psi_2''' = -\frac{\partial(\omega_0, \psi_1'')}{\partial(x,y)} - \frac{\partial(\omega_1'', \psi_0)}{\partial(x,y)}, \tag{46c}$$

with homogeneous boundary conditions for ψ_2', ψ_2'' and ψ_2'''.

As in the previous cases, (46) were solved numerically and the streamlines ψ_2', ψ_2'' and ψ_2''' so determined are plotted in figures 8(*a*), (*b*) and (*c*), respectively. It is apparent that each mode has a dominant set of closed streamlines, ψ_2' and ψ_2'' corresponding to counterclockwise flow and ψ_2''' to clockwise circulation. In addition ψ_2'' exhibits a weak clockwise circulation for $x > 1$. It is significant that ψ_2'' and ψ_2''' are two orders of magnitude smaller than ψ_2', since, unless $Pr \ll 1$, ψ_2 (and therefore ω_2) will always be dominated by ψ_2' (and ω_2').

In principle, it is possible to continue generating higher-order corrections to the stream-function and temperature profiles in the end region. However, with each higher-order term, the number of numerical solutions that must be calculated increases substantially. In fact, for the $O(A^n)$ problem, one must obtain $2n-1$ numerical solutions. Because of the symmetry properties of the previously obtained numerical solutions, the $O(A^4)$ problem (which has not been specifically outlined) does not contribute to K_1 (i.e. $c_5 \equiv 0$). Hence, in order to obtain the next non-trivial correction to the temperature gradient in the core ($O(Gr^4 Pr^4 A^5)$), one must proceed to the $O(A^5)$ problem in the end region. Since 13 additional solutions would be required fully to determine c_6, we have elected to terminate the asymptotic expansion at $O(A^3)$. The implications of the results to this order are discussed in the next section.

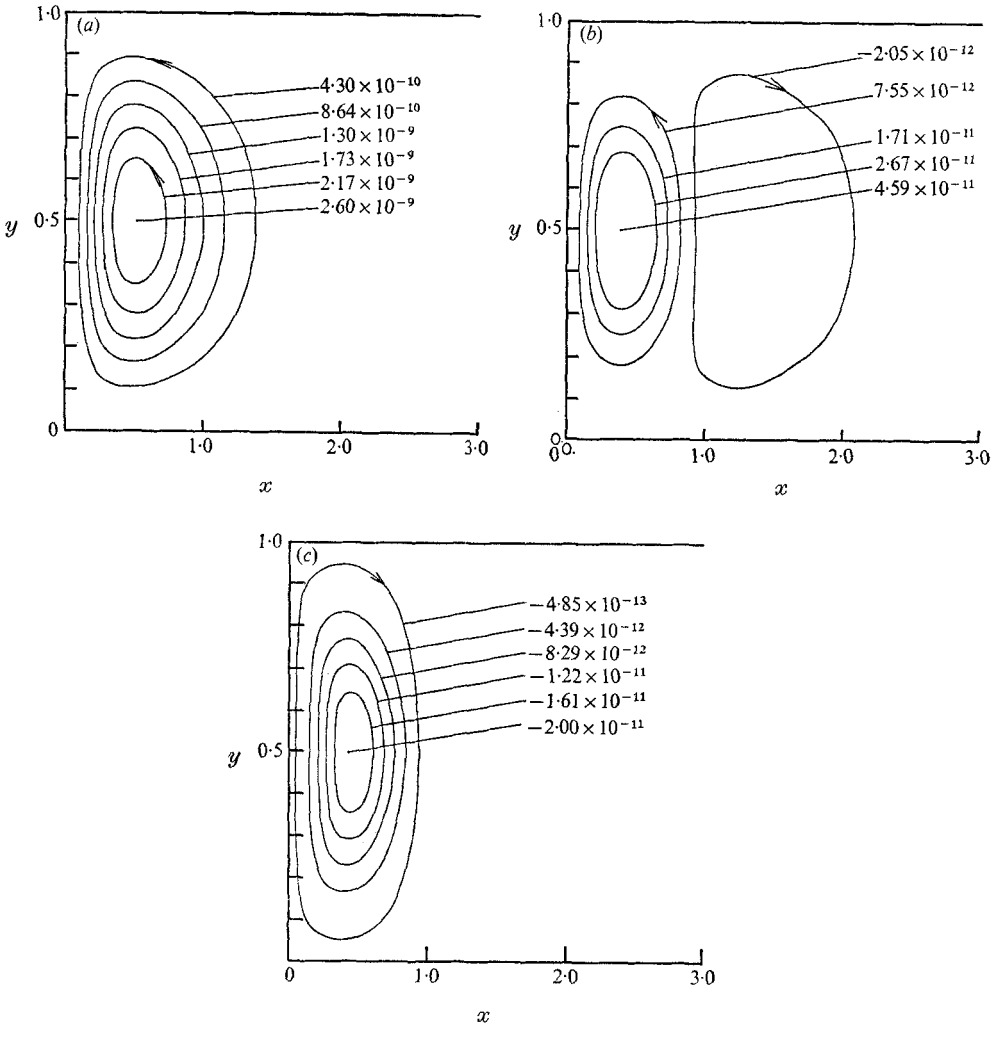

FIGURE 8. (*a*) $O(Pr^2\,Gr^2\,A^2)$ stream-function correction ψ_2', (*b*) $O(Pr\,Gr^2\,A^2)$ stream-function correction ψ_2'' and (*c*) $O(Gr^2\,A^2)$ stream-function correction ψ_2'''.

The composite expansion for the end region

To obtain a qualitative appreciation of the influence of the higher-order corrections ψ_1 and ψ_2 on the flow characteristics in the end region, we have plotted ψ_0 as well as the composite functions

$$\Psi_1 = \psi_0 + Pr\,Gr\,A\psi_1' + Gr\,A\psi_1'', \tag{47a}$$

$$\Psi_2 = \Psi_1 + Pr^2Gr^2A^2\psi_2' + PrGr^2A^3\psi_2'' + Gr^2A^3\psi_2''' \tag{47b}$$

in figure 9 for the representative parameter values $Gr = 8\times10^3$, $Pr = 6{\cdot}983$ and $A = 0{\cdot}01$. For these values, the correction terms in (47) are approximately one order of magnitude smaller than ψ_0. Hence, a good qualitative idea of the influence of each correction can be deduced, although higher-order terms

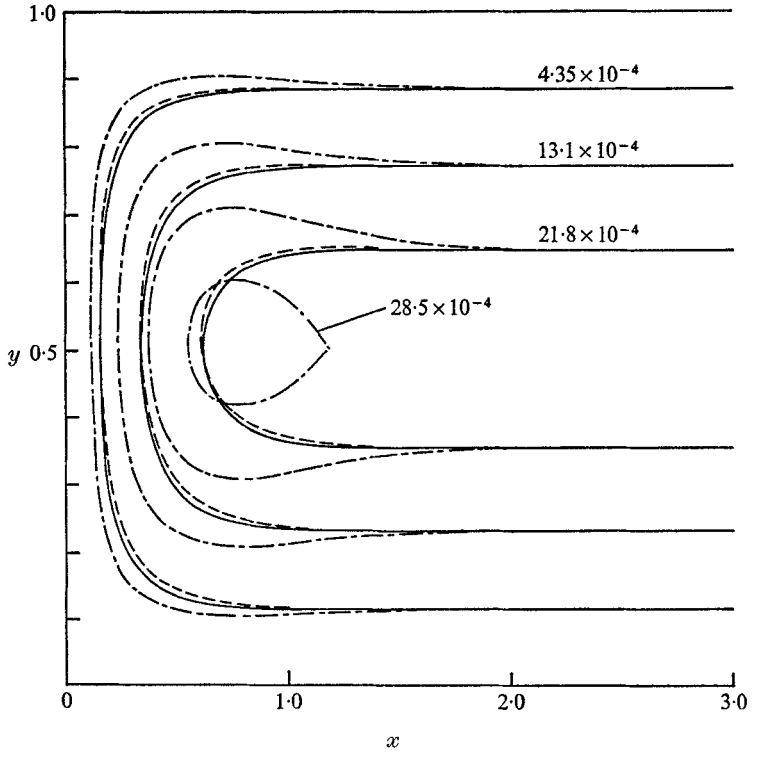

FIGURE 9. Comparison of streamlines of composite functions Ψ_1 and Ψ_2 with ψ_0. ——, ψ_0; – – – –, Ψ_1; ———, Ψ_2.

may still have an appreciable influence on any quantitative comparison between the asymptotic and exact (numerical) solution for this parameter range.

With the above limitation in mind, we note that the dominant qualitative effect of the first correction is to skew the streamlines in the cold end of the box upward relative to the symmetric function ψ_0. That is, the streamlines entering the cold end region advance further into the upper corner and are then deflected outwards to a more gently rounded corner at the bottom by the action of the end wall.

This shift in the streamlines represents the first effects of the stable stratification on the flow in the end region. A possible physical explanation is that the stratification retards vertical motion so that the fluid starts its downward flow nearer the end wall where the stratification is weakest owing to the end-wall cooling.

For particular values of the parameters considered, the second correction ψ_2 has an even more pronounced influence on the contour lines than does the first correction. (In the asymptotic limit as $A \to 0$, of course, the first corrections will be larger than the second corrections.) The influence of ψ_2 on the flow is to increase the net local mass flux. Figure 9 indicates that this increased mass flux may result in closed streamlines in the end region. The parallel streamlines that leave the core are diverted towards the upper wall and away from the lower wall

as they traverse the end region. The characteristic 'bump' in the streamlines which results is a prominent feature of the numerical results of part 2.

The value which we have used for Pr in the composite expansion of figure 9 is approximately that for water. As we have noted previously, the corrections ψ_1'', ψ_2'' and ψ_2''' become appreciable only as Pr becomes very small. Clearly, in view of the form of ψ_1'' and ψ_2''', the detailed nature of the end-region flow will be considerably modified in the limit as $Pr \to 0$. In particular, instead of the upward shift of the streamlines which we observed for $Pr = O(1)$, the streamlines in the cold end of the cavity will be shifted downwards for $Pr \ll 1$. In addition, the end-region flow will be characterized by the absence of any closed streamlines.

5. Further discussion of results

One of the main goals of theory and experiment for cavity flows is the prediction or correlation of the Nusselt number, the dimensionless heat transfer rate

$$Nu = \int_0^1 \frac{\partial \theta}{\partial x}\bigg|_{x=0} dy, \tag{48}$$

as a function of Gr, Pr and A. Such correlations have generally been deduced either from the results of many numerical solutions of the full Navier–Stokes equations (cf. Newell & Schmidt 1970) or from the results of numerous experiments.

It is possible to obtain an expression for the Nusselt number from the present asymptotic approach for the limit $A \to 0$ with Pr and Gr fixed. To obtain the relationship, we must evaluate (48) using the temperature profile in the cold end of the cavity, correct to $O(Gr^2 Pr^2 A^3)$, e.g.

$$\theta = Ax + Gr\,Pr\,A^2\theta_2' + Gr^2\,Pr^2\,A^3\theta_3' + Gr^2\,Pr\,A^3\theta_3''. \tag{49}$$

Owing to the antisymmetry of θ_2' about $y = 0{\cdot}5$ evident in figure 4, θ_2' does not contribute to the integral (48). Similarly, θ_3'' does not contribute to the integral. The contribution of θ_3', on the other hand, must be determined by numerical integration of the previously calculated distribution of θ_3'. Correct to $O(Gr^2 Pr^2 A^3)$ the result is

$$Nu = A(1 + 2{\cdot}86 \times 10^{-6} Gr^2 Pr^2 A^2).\dagger \tag{50}$$

The Nusselt number, as defined by (48), is equivalent to the longitudinal dispersion rate which is frequently used to characterize real estuaries. It is, therefore, significant that the first convective contribution to Nu is precisely the Taylor dispersion coefficient, calculated using the first-order core velocity profile (cf. equation (12) of the recent review paper of Fischer (1973)).

At the present time, there exist no experimentally or numerically determined correlations for Nu, that are valid for $A \ll 1$, with which (50) may be compared. However, it will be shown in part 2 that values of Nu calculated from numerical solutions of the full Navier–Stokes equations for $0{\cdot}1 < A < 0{\cdot}05$

† The next correction to Nu arises from the $O(A^4)$ problem and can be shown to be $c_4' Gr^2 Pr^2 A^4$.

agree with (50) provided only that $Gr^2 Pr^2 A^3$ is suitably restricted in magnitude. A point of some interest with regard to (50) is the graphic illustration it provides of the fundamental difference between the limiting processes $A \to 0$, $Gr \gg 1$ (fixed) and $A \ll 1$ (fixed), $Gr \to \infty$. In the latter circumstance we have previously suggested (and our numerical and experimental results of parts 2 and 3 provide further evidence in corroboration) that the flow structure will be dominated by natural-convection boundary layers at the side walls, with all of the horizontal temperature drop occurring in these regions and the interior core flow driven primarily by the entrainment–detrainment process associated with these layers. In this case, the Nusselt number (48) must clearly be proportional to Gr^m, with $m > 0$. In contrast, however, the expression (50) shows that, if Gr is held fixed and A is decreased without limit, the Nusselt number must ultimately become independent of Gr to first order, no matter how large Gr may be!

Finally, although the asymptotic analysis which we have considered is strictly valid only in the limit $A \to 0$ with Gr and Pr fixed, it is useful to consider the range of values of these parameters where the results may be of practical use. Such an undertaking is, perhaps, particularly desirable in the present circumstance since (14) and (15) indicate the existence of a parallel flow structure to all orders of magnitude in A. Certainly the asymptotic treatment does not explicitly indicate an upper limit of A. However, the numerical solution for ω_0, figure 2(*b*), indicates that the equi-vorticity lines are graphically parallel only for $x > 2$. Thus, before parallel flow can exist, the cavity must be at least four times as long as it is deep, or $A \lesssim 0{\cdot}25$. The form found for K_1, e.g.

$$K_1 = 1 + c_4' Gr^2 Pr^2 A^3 + O(Gr^4 Pr^4 A^5),$$

indicates that the actual value of A necessary for the core solution (14) and (15) to be valid must depend explicitly upon the fixed values of Gr and Pr. Although a rigorous convergence criterion is not possible with the limited results presented here, an approximate criterion can be obtained by requiring only that the second term in the expansion for K_1 be small relative to the first. If we take 0·1 to be small, then it is found that

$$Gr^2 Pr^2 A^3 \lesssim 10^5. \tag{51}$$

Even if the 'small' correction were allowed to be $O(1)$, the range of values of Gr, Pr and A encompassed by (51) would not be changed substantially. It is, of course, necessary to examine experimental results and/or numerical solutions of the full Navier–Stokes equations in order to substantiate the estimate embodied in (51). This we do in parts 2 and 3 of the present work.

This work was done, in part, while J. Imberger was a visitor to the Keck Laboratory of Environmental Engineering at the California Institute of Technology, with the support of a National Science Foundation Grant GK-35774X.

REFERENCES

BATCHELOR, G. K. 1954 *Quart. Appl. Math.* **12**, 209.
BENTHEM, J. P. 1963 *Quart. J. Mech. Appl. Math.* **16**, 413.
CORMACK, D. E., STONE, G. P. & LEAL, L. G. 1974 *Int. J. Mass Heat Transfer*, to appear.
DE VAHL DAVIS, G. 1968 *Int. J. Heat Mass Transfer*, **11**, 1675.
ELDER, J. W. 1965 *J. Fluid Mech.* **23**, 77.
FADLE, J. 1941 *Ing. Archiv.* **11**, 125.
FISCHER, H. B. 1973 *Ann. Rev. Fluid Mech.* **5**, 59.
GILL, A. E. 1966 *J. Fluid Mech.* **26**, 515.
MITTLEMAN, B. S. & HILLMAN, A. P. 1946 *Math. Tables & Other Aids to Comp.* **2**, 61.
NEWELL, M. E. & SCHMIDT, F. W. 1970 *J. Heat. Transfer*, **92**, 159.
QUON, C. 1972 *Phys. Fluids*, **15**, 12.
SZEKELY, J. & TODD, M. R. 1971 *Int. Heat Mass Transfer*, **14**, 467.
WILKES, J. O. & CHURCHILL, S. W. 1966 *A.I.Ch.E. J.* **12**, 161.